Article citation info:
Szwajca F, Pajor Ł, Pielecha I, Marcisz G. Transient combustion behaviour of a high-performance W12 twin turbo spark ignition drift car spec engine. Combustion Engines. 0000;XXX(X):xx-xx. https://doi.org/10.19206/CE-222701

Filip SZWAJCA
Łukasz PAJOR
Ireneusz PIELECHA
Grzegorz MARCISZ

Combustion Engines
Polish Scientific Society of Combustion Engines

Transient combustion behaviour of a high-performance W12 twin turbo spark ignition drift car spec engine

ARTICLE INFO

Received: 6 March 2026
Revised: 21 April 2026
Accepted: 31 May 2026
Available online: 6 July 2026

The paper presents an analysis of indicators of a high-performance W12 twin-turbo engine used in drifting applications, supplemented with time-series data on engine parameters. The tests were conducted on a chassis dynamometer using indicating and data logging equipment. The engine external characteristics were determined, yielding 898 kW and 1488 Nm. To enable safe in-cylinder pressure measurements, the turbocharger boost control duty cycle was limited to 30%, resulting in reduced thermodynamic loading without compromising the representativeness of the combustion process. The 450 consecutive operating cycles were recorded under transient conditions. Under full-load conditions, the average MBF50 = 13.8°CA and COV(MBF50) = 17.3%, indicating conservative phasing relative to MBT and significant cycle-to-cycle variability. It was demonstrated that indexing enables precise correlation of transient parameters with combustion evolution and is an effective tool for optimizing the calibration of high-performance engines.

Key words: *high-performance engine, dyno testing, engine indication, data logging, boost control*

1. Introductions

Currently, combustion engines remain the dominant power source in most machines, vehicles, and other means of transport. The development of the engine sparked the automotive industry's dynamic growth, and the widespread use of cars led to the emergence of a new competitive discipline: motorsport. Consequently, the internal combustion engine became one of the key areas of technological development and the main object of design competition.

Originally, motorsport was based mainly on commercial vehicles that were only slightly modified, and competition took the form of races between designated destinations or on closed-circuit tracks. Along with the development of automotive technology, numerous motorsport disciplines began to separate (Fig. 1), and vehicle designs became increasingly specialized and designed for specific competition conditions.

The construction of internal combustion engines used in motorsports differs significantly from that of commercial engines. These differences arise from distinct operating conditions and regulatory constraints. The design and operating characteristics of such engines are closely tailored to the specific discipline, and the main design differences include, among others, forced induction systems, lubrication systems, construction materials, and combustion control strategies. In the highest categories of circuit racing and single-seater, such as Formula 1, Formula 2, Formula 3, Hypercar in the FIA World Endurance Championship, and IndyCar, prototype engines are used that are designed from scratch for a specific vehicle and technical regulations [8, 24, 26, 36, 39].

The development of a prototype motorsport engine involves concept definition in accordance with technical regulations, followed by computer-aided design (CAD) as well

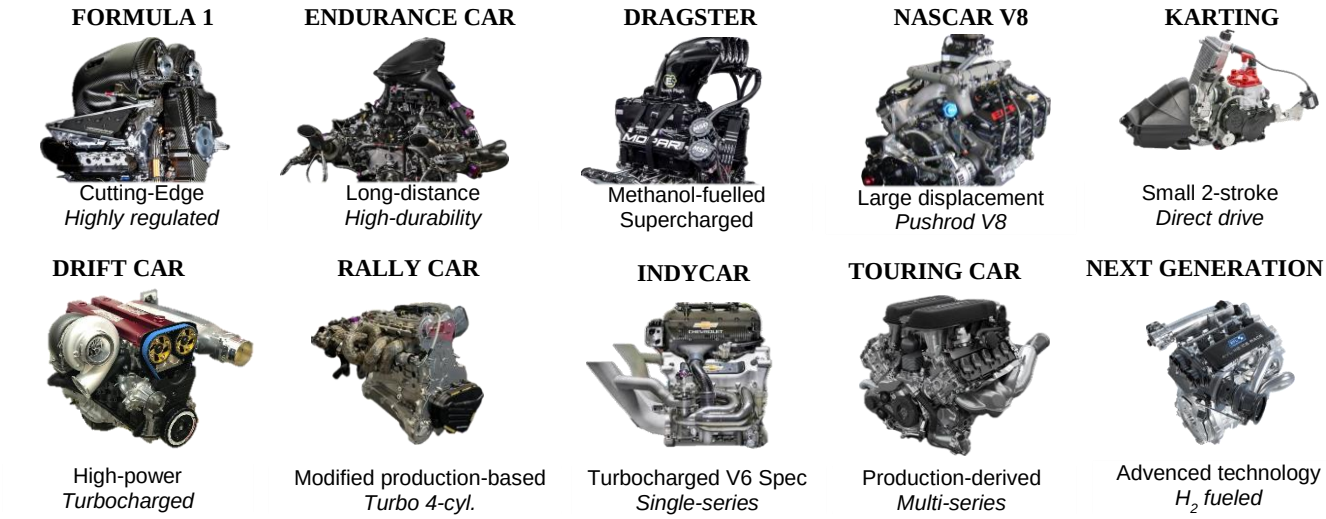

Fig. 1. Representative engine configurations used in competitive motorsport applications [5, 6, 19, 25, 29, 30, 33–35, 38]

as finite element method (FEM) and computational fluid dynamics (CFD) analyses of the engine and its components. The next step is to build a prototype and conduct tests on an engine dynamometer, including data acquisition during operation. After integration with the vehicle, development is iterative and data-driven, based on experimental data and subsequent design modifications [1]. Factory engine development programs incur extremely high costs, reaching $1.4 billion [37] in F1 and $200 million [12] in LMP1.

These costs often contribute to the decline of a racing series. An example of this is the final phase of the Class 1 regulations of the Deutsche Tourenwagen Masters series, which saw a marked escalation in the technical sophistication of the vehicles, directly translating into increased participation costs [15].

The cars were equipped with carbon monocoques and highly powerful, prototype 2.0 L R4 turbo engines (BMW P48, Audi 2.0 L R4 TFSI DTM), designed from scratch as structural elements of the vehicle (Audi RS5 DTM – Fig. 2) [10, 27].

The use of such advanced designs significantly increased development and operating costs to a level comparable to other top series based on prototypes. For comparison, the estimated budgets for the Audi and BMW factory programs for car construction in the final phase of the Class 1 regulations were around €30–50 million per year [14].

Fig. 2. Fully prototype, centrally single-seat carbon-monocoque Audi RS5 DTM [3]

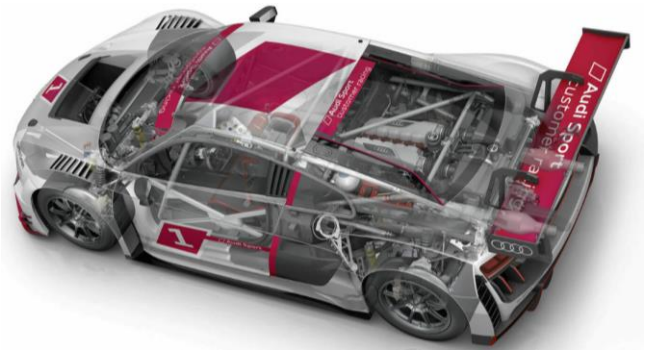

Fig. 3. Production-based Audi R8 LMS GT3 with a series-derived V10 and race-modified suspension [4]

In contrast, in the first season of the new regulations, they could reach as much as €80 million. The DTM program for private teams was estimated at €5–6 million per year [14]. Following the rule changes from the 2021 season, which allowed only FIA GT3 cars with production-derived powertrains (including the BMW S58 inline six-cylinder, the naturally aspirated Audi R8 LMS V10 (Fig. 3), and Mercedes-AMG V8 units) and the simultaneous application of the Balance of Performance system, budget requirements have decreased to around €3 million. The number of competitors has increased to around 24 [20].

Engines prepared for drifting and lower-level touring car series, such as TCR, GT, and NASCAR, as well as for selected national single-seater applications, use production-based engines due to limited budgets [20]. Using ready-made engines allows skipping many R&D stages, limiting engine preparation to modifications to the equipment and control system.

Drifting is a relatively new discipline, in which mainly private competitors participate, or factory support is only available in the highest class of formula drift (Papadakis Racing supported by Toyota Gazoo Racing [32], Ford Racing support for Vaughn Gittin Jr, Chelsea DeNofa, and most recently, James Dean [16]), which significantly affects much smaller budgets and access to factory programs.

In drift racing, the engine is exposed to frequent dynamic loads, where quick throttle response, high torque across a wide range of engine speeds, and the ability to maintain stable operation under non-steady flow and cooling conditions are crucial. Unlike factory motorsport programs, where engine dynamometers and indicator measurements are the primary tools for engine development, in drifting projects based on modified production engines, the process of validation, tuning, and performance control is usually limited to a chassis dynamometer, less often to an engine dynamometer, and advanced indicator testing is rare.

Drifting designs most often use engines derived from high-performance production models, such as the Toyota 2JZ-GTE and Nissan RB26DETT inline six-cylinder engines, modern BMW R6 engines (e.g., S55/S58), or naturally aspirated and supercharged V8s from the GM LS family, which, thanks to their rigid block architecture and high availability of parts, provide a convenient base for competitive applications [13]. In adapting production engine blocks for motorsport applications, it is crucial to increase structural rigidity and resistance to high thermal and mechanical loads. Among other things, open-deck blocks are pinned to stabilize the cylinder liners, and additional reinforcements are added to the lower part of the engine in the form of girders or stiffening plates for the crankshaft supports [22]. These design changes are often complemented by advanced functional coatings, such as ceramic thermal barrier coatings (TBCs) applied to piston crowns and low-friction coatings (LFCs) used on piston skirts or bearing surfaces, which reduce friction losses and improve durability under high-load operating conditions [17, 40].

An integral part of the powertrains used in drifting is forced induction, which allows for very high specific power while maintaining a wide torque range. In practice, single-turbocharger systems or high-performance twin-turbo configurations offering high mass flow rate and high pressure ratio (Garrett G40/G42, BorgWarner EFR 9280) dominate.

The construction of the high-performance ERF series turbocharger equipped with advanced regulation and control systems is shown in Fig. 4. The performance map of the 9280 model (Fig. 5) demonstrates the capability to achieve pressure ratios exceeding 4.0 and airflow rates above 100 lb/min, significantly higher than those typical of standard passenger-car turbochargers.

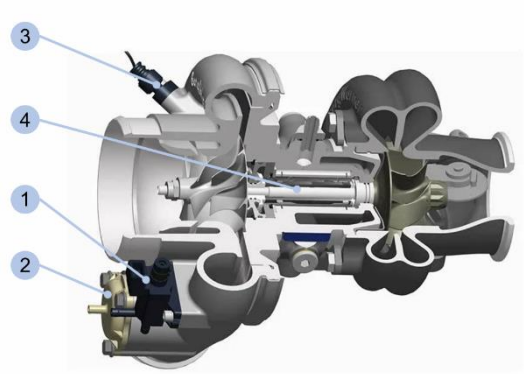

Fig. 4. Construction of twin scroll BorgWarner EFR series turbocharger, equipped with a boost pressure control solenoid valve (BCSV) (1), integrated compressor bypass valve (CRV) (2), rotor speed sensor (3), and ceramic ball bearings (4) [18]

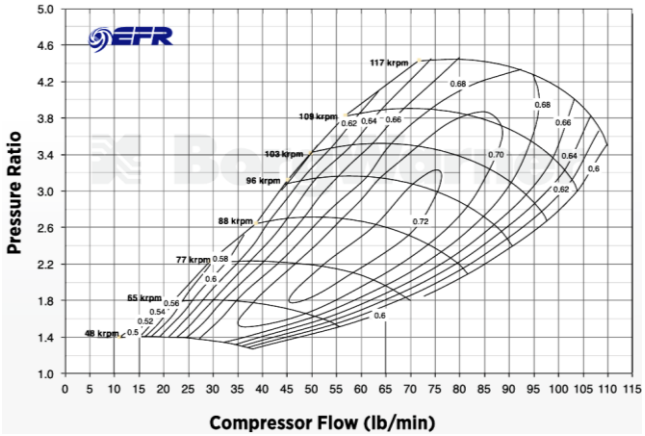

Fig. 5. BorgWarner EFR 9280 turbocharger compressor performance map [9]

At the same time, mechanical compressors are used much less frequently and are mainly found in selected projects based on V8 engines. The most commonly used turbochargers are those with ball bearings and twin-scroll housings, working with equal-length exhaust manifolds and external wastegates [28]. Blow-off valves are used on the compressor side to limit surge during rapid throttle closure.

In addition to a reinforced engine housing and a high-capacity turbocharging system, a control system based on programmable standalone ECUs with individual electrical harnesses is required. The official controller used in the Formula Drift series is Link ECU [23], but in practice, teams also use other programmable standalone units such as MoTeC, ECUMaster, Haltech, and AEM [11]. These solutions are essential in drifting – they provide full control over engine operation and the implementation of motorsport strategies such as flex-fuel using an ethanol content sensor, anti-lag and launch control systems for better use of forced induction, advanced engine thermal management and lubrication control strategies, as well as extensive data recording and integration with additional vehicle systems [2].

In addition to the three fundamentals of a drifting engine described above, independent cooling and lubrication systems play an important role in maintaining stable engine operating conditions under prolonged loads and during high-lateral-force driving.

In practice, complex oil-cooling systems, electric cooling pumps, additional oil and coolant radiators, and larger oil pans or dry-sump systems are used to prevent temporary drops in lubrication pressure. These are complemented by reinforced ignition systems, high-performance fuel injectors, temperature and pressure sensors at key points in the engine, and ECU-protected strategies that limit torque when the permissible operating parameters are exceeded.

Drifting engine calibration is typically performed on a chassis dynamometer using a standalone ECU [7,21]. Calibration begins by setting the base Fuel Table (VE or Injector Pulse Width) and the Ignition Timing Map, then adjusting the Boost Control Table based on gear or throttle position. Under these conditions, the operating limits are determined based on parameters such as lambda target (usually $\lambda \approx 0.78–0.85$ at high load), exhaust gas temperature (EGT), knock level, intake air temperature (IAT), and torque values, with ignition and fuel dose adjustments made iteratively based on ECU logs. After dyno calibration, motorsport strategies are implemented, including Anti-Lag Control, Launch Control, Gear-based Boost, and Ignition Cut during gear changes, with final tuning taking place under track conditions through analysis of telemetry data and correction maps.

Typically, drifting engines are tuned without indicator measurements, which is why the unit's operating limits are determined based on indirect indicators available in the ECU and on a chassis dynamometer [31]. Ignition calibration is performed using the "torque plateau" method, which involves gradually increasing the ignition advance angle until the torque increase disappears, while observing the knock level, exhaust gas temperature and lambda stability. In the absence of parameters such as MBF50, APmax, or MAPO, tuners rely on analyzing logs covering knock retard, speed increase, intake air temperature, and ignition corrections to determine a safe operating margin for the engine. However, this does not guarantee maximum thermodynamic efficiency.

Considering the limited scope of thermodynamic research on this type of design (motorsport drifting ICE +1000 HP), the authors decided to conduct experimental verification and identification tests involving indicator measurements, enabling direct analysis of the combustion process in the cylinder and engine operating parameters. Comparing the indicator results with the ECU operating data enables an assessment of the impact of the adopted tuning strategies on combustion-chamber processes and indicates potential directions for further modification of the drive unit.

2. Engine and test object description

The research subject was a high-performance race engine built by Gregor Performance for drifting-type competi-

tion. The engine was based on a W12 spark ignition engine with twin turbochargers. The tested engine was installed in a Nissan 350Z (Z33) body, fully prepared for motorsport (Fig. 6). The aim of the modification was to achieve a high engine power output under specific racing operating conditions.

The engine technical data are presented in Table 1. The main features include a 48-valve DOHC system, PFI (port fuel injection), and a dry-sump lubrication system. Forced induction was achieved via a twin-turbo system with Garrett GT35 units. The engine was controlled by two independent Ecumaster EMU Black controllers. This standalone solution allowed for the operation of 12 cylinders.

Table 1. High-performance drift car Engine specifications

Parameter	Value
Engine type	W12 | DOHC | PFI
Displacement	5998 cm³
Number of valves per cylinder	4
Cylinder bore	84.0 mm
Piston stroke	90.2 mm
Compression ratio	10:1
Engine aspiration	twin-turbo aspirated engine

a)

b)

Fig. 6. Drift-spec Nissan 350z (a) with W12 high-performance engine (b)

A security algorithm based on knock detection, exhaust gas temperature control, mixture composition, and oil pressure was used. The fuel system was adapted to operate in Flex Fuel mode based on alcohol concentration measurements in the fuel. The engine control system is adapted to high-octane gasoline, alcohol fuels, and mixtures (E85). The engine temperature was regulated by an independent cooling system. System output was regulated by EWP electric pumps, which were controlled directly by the ECU. The drive train is based on a modified ZF 8HP eight-speed transmission, controlled by an external standalone controller. This control method enabled independent management of the gear shift strategy. The tests were conducted with E85 racing fuel, and the fuel composition sensor indicated an ethanol content of 69%.

3. Experimental setup and research methodology

3.1. Engine dynamometer test bench

The engine tests were carried out on a hub dynamometer test bench (Fig. 7).

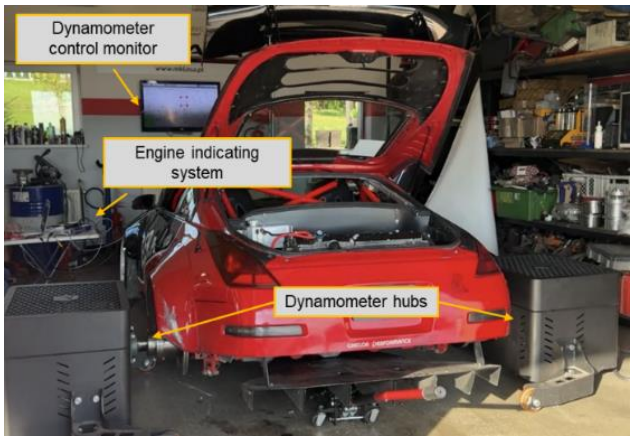

Fig. 7. Vehicle mounted on a chassis dynamometer during experimental testing under real load conditions

The specific characteristics of the test bench enabled the elimination of undesirable wheel slip. It is particularly important when testing engines that generate high torque. The Dyno Revolt HR-2 dynamometer was employed, enabling torque measurements in the 0–4000 Nm ±0.1% FS and wheel rotational speed 0–3500 rpm. The dynamometer measuring range enabled stable testing across the entire engine operating range. The combustion engine was tested on a chassis dynamometer during the car's operation. That enabled simultaneous acquisition of indicator parameters and powertrain operating values under real load conditions.

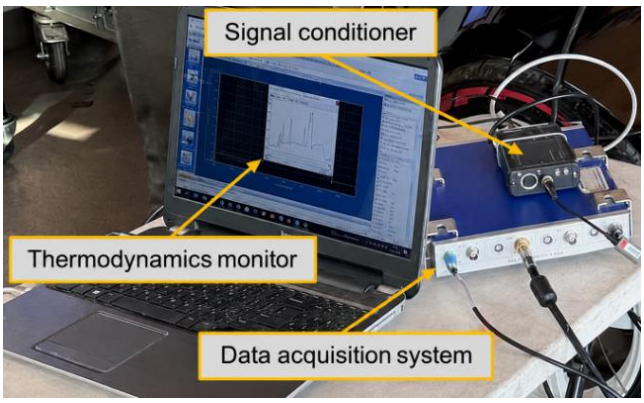

Fig. 8. View of AVL data acquisition system for thermodynamic combustion process analysis

3.2. Data acquisition system and measurements apparatus

The AVL IndiMicro 602, a four-channel system dedicated to the analysis of in-cylinder processes (Fig. 8), and an EcuMaster EDL-1 data logger were used to record data. The indicator measurement system for the crankshaft angular position included a piezoelectric pressure transducer integrated with an AVL ZI45 spark plug, a Pico TA398 high-voltage probe, and Pico TA018 current clamps. The cylinder pressure, high voltage in the secondary circuit of the ignition coil, and the injection control current were recorded. All measurements were performed within a single engine cylinder. Engine operating parameters were acquired from time traces using a dedicated data logger connected to the ECU. A total of 32 parameters were selected for recording, with a sampling frequency of 25 Hz. The specifications of the measuring equipment used are presented in Table 2.

Table 2. Measurement equipment and technical specifications

Parameter	Description	Specification
Combustion analysis	AVL IndiMicro 602	4 channels Δα = 0.5 °CA
Data logger	EDL-1	200 channels f_s = 25 Hz
Cylinder pressure	AVL ZI33	0–250 bar ±0.3% FS
Ignition high voltage	Pico TA398	Attenuation ratio 10,000:1
Injector signal	Pico TA018	0–60A 2.0%; ±5 mA

3.3. Experimental plan and data processing

The tests were divided into two stages. The first stage involved determining the engine's external characteristics at full boost. The second stage involved determining the external characteristics, supplemented by a thermodynamic analysis of the combustion process under limited boost (30%) to mitigate the risk of damage to the spark plug integrated with the pressure transducer. During the second stage, the engine was diagnosed at idle speed.

The processing of measurement data recorded in the crankshaft angle function began with low-pass filtering at a cutoff frequency of 4 kHz. Next, the heat dissipation characteristics were determined in accordance with a simplified model based on the first law of thermodynamics [18]:

$$\frac{dQ}{d\alpha} = \frac{\gamma}{\gamma-1} P \frac{dV}{d\alpha} + \frac{1}{\gamma-1} V \frac{dP}{d\alpha} \quad (1)$$

where: γ, the polytropy exponent, was set at 1.32 for compression and 1.27 for expansion stroke; P is the measured pressure in the cylinder, and V is the current cylinder volume relative to the angular position of the crankshaft.

Based on the current volume and pressure in the cylinder, the average indicated mean effective pressure was determined according to the formula:

$$IMEP = \frac{1}{V_d} \cdot \int PdV \quad (2)$$

where: V_d is the displacement volume, P is the instantaneous pressure value for the instantaneous cylinder volume V.

Maximum values and their angular positions were determined for selected parameters. The ignition timing SOIgn was determined from the high-voltage waveform in the secondary circuit of the ignition coil.

4. Results

4.1. Full-load engine performance characteristics

Figure 9 illustrates the full-load characteristics of the engine operating at 100% boost (solid line) and at a turbocharger boost control duty cycle limited to 30% (dashed line). Under full boost conditions, the engine produced 889 kW at 6222 rpm and 1488 Nm of torque at 4393 rpm. These results were used to limit the boost during indicator measurements. Under limited boost conditions, the engine produced 508 kW and 889 Nm of torque.

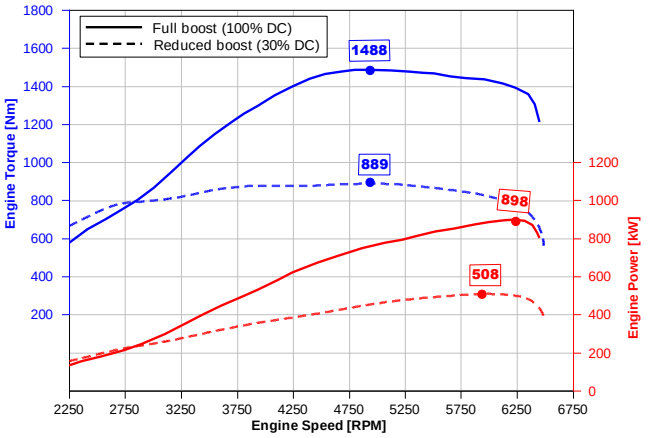

Fig. 9. Engine torque and power characteristics measured on a chassis dynamometer under full and partial boost conditions

The obtained results reflect the high-performance configuration of the tested engine, including turbocharging, a modified intake system, standalone ECU control, and operation on ethanol-blended fuel. High engine torque is required in drifting to maintain controlled rear-wheel slip during sustained oversteer conditions.

4.2. Engine control variables under test conditions

The control method is important for engine performance under the specific operating conditions dictated by motorsport. The engine calibration strategy was based on external operating parameters available from the ECU, without direct feedback from in-cylinder combustion analysis. Figure 10 illustrates the time-based selection of engine control variables and operating parameters under partial boost conditions.

Figure 10a presents the time history of absolute manifold pressure in the intake manifold (MAP) after the turbocharger (green line) and the boost control duty cycle of the solenoid valve regulating the turbocharger output flow (blue line). During the initial phase of engine acceleration and gradual throttle opening, at engine speeds from 1650 to 2400 rpm, the increase in boost pressure is regulated by the rising exhaust gas flow driving the turbine. Above 2400 rpm, the engine enters wide-open throttle (WOT), and the intake manifold pressure rises above atmospheric pressure. At the same time, the boost is limited to approximately 30%, corresponding to a partial exhaust gas bypass before the turbine blades. Despite the use of exhaust gas bypass,

further increases in engine speed result in boost pressure rising to 160 kPa, with the valve control ratio simultaneously corrected to 23%. Once the maximum engine speed of 6335 rpm is reached, the throttle closes, and the boost air relief valve takes over the boost pressure control function.

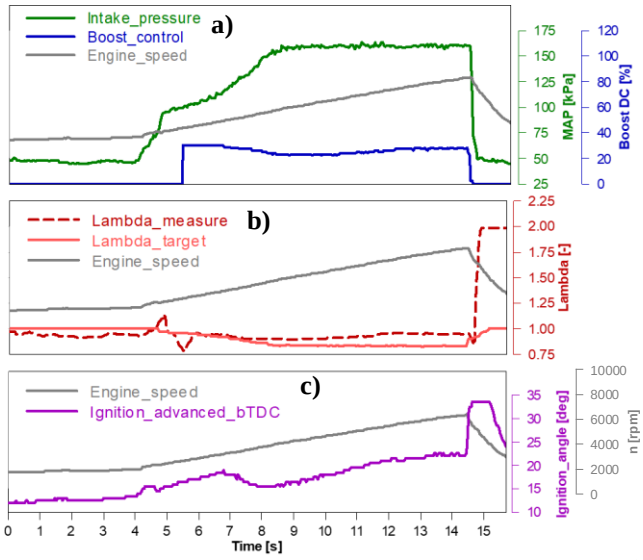

Fig. 10. Transient engine control variables and operating parameters recorded under partial boost conditions

Figure 10b shows changes in the air excess ratio λ during acceleration. The dotted line represents the actual value of λ measured by the oxygen sensor at the exhaust, while the solid line represents the value set by the engine control unit. The set value at idle speed was determined to achieve stoichiometric combustion, aiming for a rich combustion λ ≈ 0.83 during engine acceleration. The transient boost control during the initial phase of acceleration produced a temporary lean mixture with λ ≈ 1.15, followed by enrichment to λ ≈ 0.95 due to fuel metering. During further acceleration, the setpoint and actual values were the same. However, this trend changed towards running on a leaner mixture than the setpoint due to insufficient turbocharger boost control duty cycle despite the current correction from 30 to 24%, but without exceeding λ = 1.00. In the range from 1600 rpm to 3000 rpm, the ignition advance angle increased classically with rotational speed (Fig. 10c). Subsequently, up to 3900 rpm, there was a correction related to the boost limitation and a linear increase correlating with the engine speed.

4.3. Transient thermodynamic indicator analysis

The test was conducted for 0 to 15 seconds, and, in parallel with the time signal recording, a total of 450 consecutive engine cycles were recorded and presented as cylinder pressure curves (Fig. 11).

The first 70 cycles corresponded to transitional states associated with throttle opening. In this range, a gradual increase in maximum combustion pressure was observed, reaching approximately 33 bar. Cycles 70 to 197 represented the engine-load increase phase, during which maximum pressure increased to approximately 85 bar. The subsequent cycles corresponded to the engine operating at full load, characterized by relatively stable maximum pressure values.

The observed changes in cylinder pressure represent the transition from low-load operation through a phase of increasing load to stable high-load conditions.

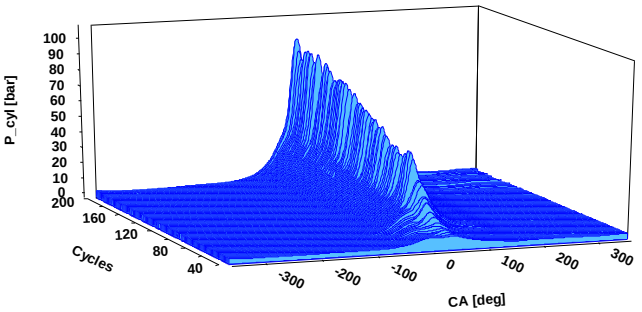

Fig. 11. In-cylinder pressure evolution versus crank angle and subsequent cycles under transient partial boost conditions

4.4. Combustion process characteristics under transient operating conditions

Based on the cylinder pressure curves, the time-dependent changes in the combustion process's characteristic parameters were determined (Fig. 12), including IMEP, Pmax, maximum heat release rate, MBF10, MBF50, and MBF90, which enabled the evaluation of combustion phasing evolution under transient engine operating conditions.

Over a period of up to 4 seconds, the engine idled at a load range of 1.2 to 1.9 bar IMEP, with a constant maximum combustion pressure of approximately 6.5 bar and a maximum heat release rate of 20 kJ/m³ °CA. Operation at the load necessary to maintain idling, despite the small variability of Pmax and dQmax, was characterized by high variability in the angle of maximum pressure APmax. The irregularity of the APmax position determined the variability in the start of combustion (MBF10), but did not significantly affect the duration of the first phase of combustion (MBF10–MBF50) or the second phase (MBF50–MBF90). It was observed that during idling, both combustion phases had a similar duration.

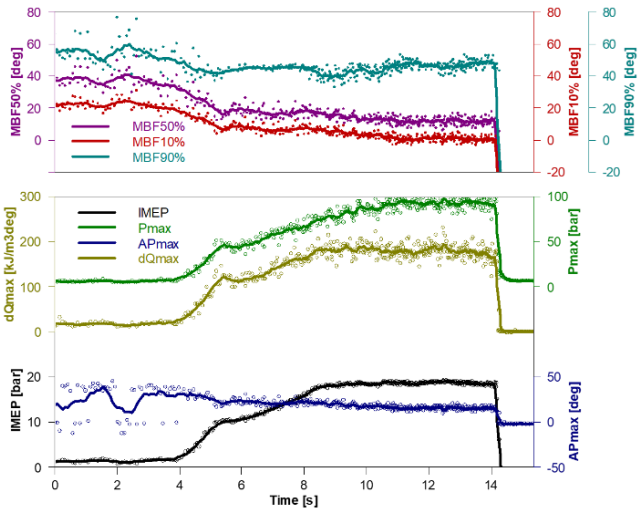

Fig. 12. Transient in cylinder thermodynamics indicators of the combustion process under partial boost conditions

The increase in engine load from 4 to approximately 8.2 s, corresponding to an increase in IMEP from 1.9 to less than 18 bar, significantly affected the stabilization of the APmax angle and the change in the share of individual combustion phases. As the load increased, the values of Pmax (up to approx. 72 bar) and dQmax (up to approx. 180 kJ/m³ °CA) increased, while the angles APmax and MBF10 accelerated systematically from 31 to 25°CA aTDC and from 16 to 7°CA aTDC, respectively. The acceleration of combustion initiation was accompanied by a corresponding shift in the MBF50 center of combustion. At the same time, an elongation of the second combustion phase from approximately 15 to 30°CA was observed, while the MBF90 angle showed an upward trend (from approx. 42°CA to 45°CA), opposite to the changes in the start and center of combustion. With increasing load, there was a clear reduction in the MBF90 spread, but not in MBF10 or MBF50.

The combustion process at full load, up to approximately 14 seconds of the test and at IMEP ≈ 18.5 bar, was characterized by roughly constant values of Pmax and dQmax, amounting to about 92 bar and 182 kJ/m³ °CA, respectively. The APmax angle accelerated further from 22 to 18.5°CA aTDC, accompanied by a shift in MBF10 from 7 to around 0°CA and an acceleration in MBF50 from 18 to 11°CA aTDC. At full load, a renewed rise in MBF90 dispersion was observed despite earlier stabilization. Full-load operation extended the second combustion phase from around 23 to 36°CA, while the first phase remained almost constant at around 11°CA.

The observed redistribution of the duration of individual combustion phases is confirmed by the analysis of pressure and heat release rate curves presented in the next subsection. Figure 13 shows the changes in the angular duration of individual combustion phases, determined from MBF curves. Blue triangles mark the MBF10–50 range, red squares mark MBF50–90, and black diamonds mark the total combustion period MBF10–90.

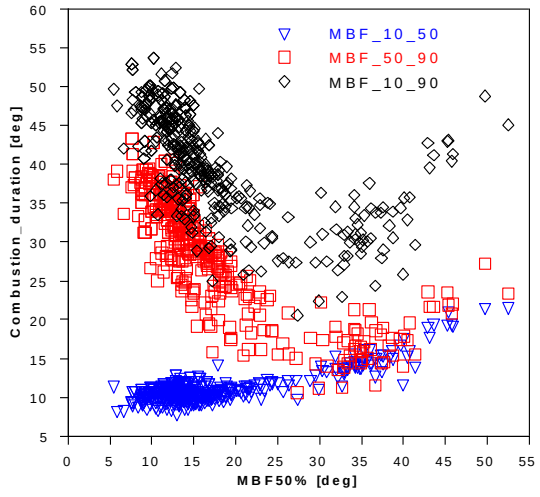

Fig. 13. Relationship between combustion duration intervals and MBF50 phasing under transient partial boost conditions

In the initial phase of engine operation, a wide spread of MBF10–90 values was observed, due to combustion instability under transient conditions. As the load increased, the total combustion time shortened gradually, and the proportion of the second combustion phase (MBF50–90) decreased markedly. At the same time, the first combustion phase (MBF10–50) showed a slight prolongation and stabilization of the course.

The observed changes indicate a transition from angularly extended combustion at low load to a more concentrated combustion at higher IMEP values.

Figure 14 shows the relationship between the selected parameter describing the combustion process and the engine operating conditions during transient states. In the initial phase, a large spread of values was observed, characteristic of unstable combustion at low load. As the load increased, the curve gradually became more orderly and shifted to a region of lower variability, corresponding to stable combustion at higher IMEP values.

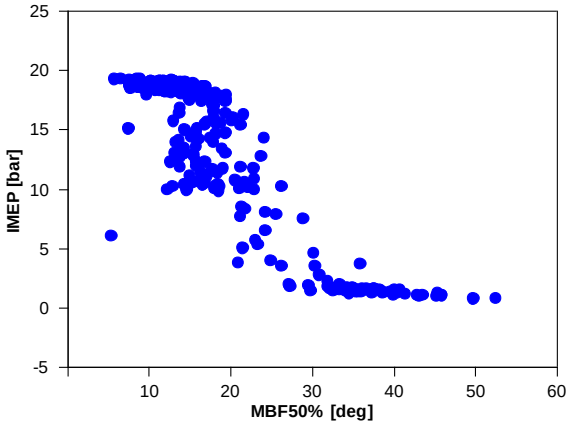

Fig. 14. Relationship between combustion duration intervals and MBF50 phasing under transient partial boost conditions

4.5. In-cylinder pressure phenomena in different states of engine operation

When the throttle was opened and the fuel dose was increased to maintain the set λ value, a gradual increase in cylinder pressure and heat release rate was observed (Fig. 15). Despite the acceleration of the ignition advance angle, the combustion process clearly proceeded after TDC, and the position of the maximum pressure angle APmax did not show a clear tendency to occur earlier. At the same time, the maximum heat release rate, dQ/dα, occurred earlier in each subsequent cycle. The visible irregularity of the dQ/dα curve indicated instability in the combustion process, characteristic of transitional states of engine operation.

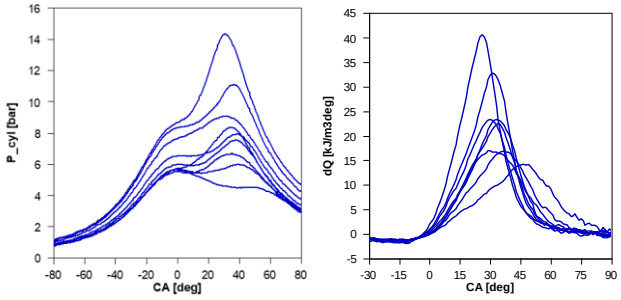

Fig. 15. In-cylinder pressure and heat release rate for selected initial acceleration cycles under partial boost conditions

A detailed thermodynamic analysis of the selected engine operating cycle at idle (Fig. 16) showed an extended discharge phase lasting approximately 11.5°CA. As a result, the combustion process was prolonged, leading to delayed combustion. This was caused by a significant proportion of combustion occurring after TDC and by an extended period of increased heat release rate. This pattern indicates the dominance of combustion initiated by ignition under conditions of heterogeneous charge preparation.

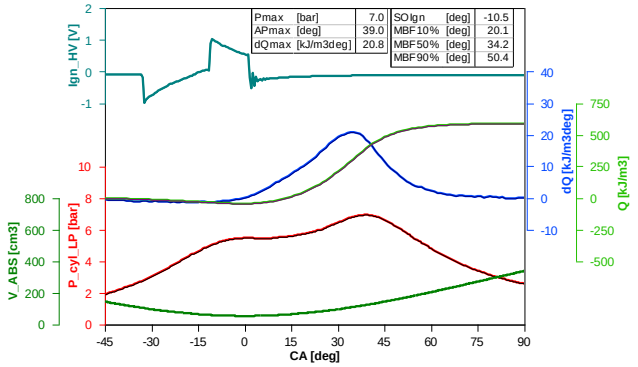

Fig. 16. Thermodynamic analysis of a representative engine cycle during idle operation

Figure 17 shows the pressure curves in the cylinder and the heat release rates for selected cycles, illustrating the changes during an increase in engine load. Increasing the load causes a clear increase in the maximum value of dQ/dα and a shift in the combustion process towards TDC. At the same time, the irregularity of the dQ/dα curves disappeared, indicating stabilization of the combustion process and a more kinetic reaction.

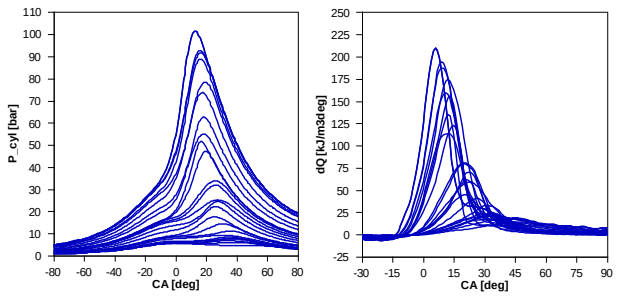

Fig. 17. In-cylinder pressure and heat release rate for selected cycles representing increasing load over the entire test

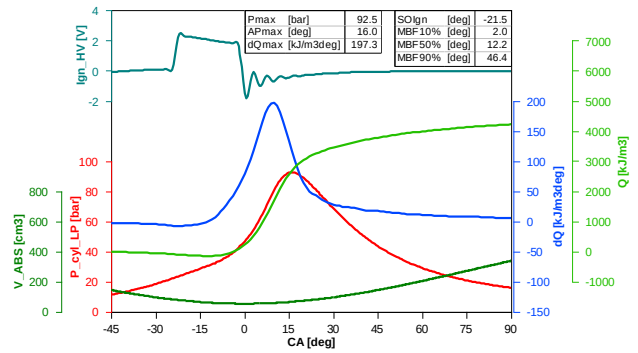

Fig. 18. Thermodynamic analysis of a representative engine cycle during full-load operation

A detailed thermodynamic analysis (Fig. 18) indicated an extension of the angular discharge period to approximately 18°CA. Combustion was kinetic, with a homogeneous mixture, and the increase in heat release rate was more rapid, although the maximum Q values were reached slightly later than in the initial acceleration phase.

5. Summary and conclusions

The performed thermodynamic indicator analysis demonstrated that in-cylinder pressure measurements constitute a significant extension of traditional motorsport engine calibration procedures. Conventional tuning based on external parameters such as torque, air–fuel ratio or exhaust gas temperature enables safe engine operation; however, it does not provide direct information about combustion phasing or thermodynamic loading of engine components. The results obtained in this study confirm that indicator measurements allow a more precise evaluation of combustion behaviour in a highly modified production-based racing engine and create a link between empirical dyno tuning and advanced experimental diagnostics. The main findings of the study are summarized as follows:

1) In the tested setup, the engine achieved 889 kW at 6222 rpm and 1488 Nm at 4393 rpm, confirming the high-performance characteristics required in drifting applications.
2) Limiting the boost control duty cycle to 30% reduced the engine output to 508 kW and 889 Nm. Under these conditions, the measured in-cylinder pressure and overall engine load were significantly lower, thereby minimizing the risk of damage to the spark plug-integrated pressure transducer during indication measurements.
3) The ability to directly link transient (temporal) parameters with the analysis of successive operating cycles was achieved, enabling the evaluation of combustion evolution during load ramp-up.
4) Under idle conditions, significant variability in the APmax angle and MBF phases was observed, with high repeatability in the heat release rate (HRR) curve.
5) Under transitional conditions, with increasing load, stabilization of the APmax angle and a reduction in MBF90 dispersion were observed, while MBF50 variability remained significant in the initial phase of load increase.
6) At full load, increased variation in maximum heat release rate (HRR) and Pmax was observed, indicating high sensitivity of the combustion process under WOT conditions.
7) In the case of traditional tuning without engine indication, at full load, an average MBF50 value of 13.8°CA was obtained, slightly delayed relative to MBT, but ensuring a safe operating margin; at the same time, COV(MBF50) = 17.3% indicated significant cycle-to-cycle variability. The use of indicator-based tuning could bring the combustion phasing closer to MBT and reduce uniqueness at maximum IMEP and WOT.
8) Engine tuning is a significant extension of traditional calibration methods, enabling improved tuning quality, increased combustion process repeatability, and potential improvements in engine performance and stability.

Acknowledgements

This work was carried out as part of the author's Bachelor's thesis at the Faculty of Civil and Transport Engineering. The research was conducted with the support of Gregor Performance Garage and M. Klasa Motorsport Electronics.

Nomenclature

APmax	angle of maximum in-cylinder pressure
aTDC	after top dead centre
BDC	bottom dead centre
CAD	computer-aided design
CI	compression ignition
CNG	compressed natural gas
COV	coefficient of variation
DI	direct injection
DOHC	double overhead camshaft
DTM	Deutsche Tourenwagen Masters
ECU	engine control unit
EGT	exhaust gas temperature
FIA	Fédération Internationale de l'Automobile
GT3	Grand Touring class 3
HRR	heat release rate
ICE	internal combustion engine
IMEP	indicated mean effective pressure
IAT	intake air temperature
LMP1	Le Mans Prototype 1
MAP	manifold absolute pressure
MAPO	maximum amplitude of pressure oscillation
MBF	mass burn fraction
MBT	minimum advance for best torque
PFI	port fuel injection
Pmax	maximum in-cylinder pressure
SI	spark ignition
SOC	start of combustion
TCR	Touring Car Racing
TDC	top dead centre
WOT	wide open throttle

Bibliography

[1] Alten H, Illien M. Demands on Formula One engines and subsequent development strategies. SAE Technical Paper 2002-01-3359. 2002. https://doi.org/10.4271/2002-01-3359

[2] ASM Tuning. Piggyback vs. Standalone ECU. 2026. https://asmtuning.co/piggyback-vs-standalone-ecu/

[3] Audi MediaCenter. DTM 2019 – photo detail. 2026. https://www.audi-mediacenter.com/en/photos/detail/dtm-2019-82435

[4] Audi MediaCenter. Audi R8 LMS – photo detail. 2026. https://www.audi-mediacenter.com/en/photos/detail/audi-r8-lms-20153

[5] AutoRacing1. IndyCar 2.4L engines developed by Chevy and Honda headed to scrap heap. 2023. https://www.autoracing1.com/pl/389824/indycar-2-4l-engines-developed-by-chevy-and-honda-headed-to-scrap-heap/

[6] AVL RaceTech. Vehicle and propulsion – H2 Race Engine. 2026. https://www.avlracetech.com/vehicle-and-propulsion

[7] Banish G. Engine management: advanced tuning. CarTech Inc.; 2011.

[8] Boretti A. Prototype powertrain in motorsport endurance racing. Warrendale, SAE International; 2018. https://doi.org/10.4271/PT-185

[9] BorgWarner I. Turbo performance catalog. Auburn Hills (MI): BorgWarner Inc. 2024. https://www.borgwarner.com/docs/default-source/iam/boosting-technologies/bw_turbo-performance-catalog.pdf

[10] Budack R, Wurms R, Mendl G, Heiduk T. Der neue 2,0-l-R4-TFSI-Motor von Audi. MTZ – Mot Z. 2016;77:16-25. https://doi.org/10.1007/s35146-016-0035-2

[11] Chiriac R-L, Chiru A, Boboc RG, Kurella U. Advanced engine technologies for turbochargers solutions. Appl Sci. 2021;11:10075. https://doi.org/10.3390/app112110075

[12] Dagys J. Juttner: LMP1 Hybrid is "Overkill" for Costs, Sustainability. 2017. https://sportscar365.com/lemans/wec/juttner-costs-for-lmp1-hybrid-is-overkill/

[13] Engine Builder. Smoking Tires: A Look Inside Formula Drift. 2020. https://www.enginebuildermag.com/2021/09/smoking-tires-a-look-inside-formula-drift/

[14] Errington T. Audi aiming to reduce its DTM budget in 2020. MotorsportCom. 2019. https://www.motorsport.com/dtm/news/audi-reduce-budget-2020-gass/4547683/?utm_source=chatgpt.com

[15] Euwema D. DTM unveils GT3-based regulations and 2021 calendar. 2020. https://www.motorsportweek.com/2020/11/06/dtm-unveils-gt3-based-regulations-and-2021-calendar/

[16] Ford Racing. Ford Motorsport – drifting. 2026. https://www.fordracing.com/motorsport/drifting

[17] Gautam SS, Singh R, Vibhuti AS, Sangwan G, Mahanta TK, Gobinath N, et al. Thermal barrier coatings for internal combustion engines: a review. Mater Today Proc. 2022;51:1554-1560. https://doi.org/10.1016/j.matpr.2021.10.371

[18] GCG. All you need to know – BorgWarner EFR turbochargers. 2024. https://gcg.com.au/latest-news-details/All-You-Need-To-Know-BorgWarner-EFR-turbochargers-news.html

[19] Goodwin G. Toyota release TS050 powertrain images. 2024. https://www.dailysportscar.com/2019/10/04/toyota-release-ts050-powertrain-images.html

[20] Haidinger S. This is how much it costs to race a full DTM season. 2026. https://www.motorsport.com/dtm/news/how-expensive-is-it-to-compete-in-a-dtm-season/10788662/

[21] Hartman J. How to tune and modify engine management systems. MotorBooks International; 2004.

[22] Hoag K, Dondlinger B. Cylinder block layout and design decisions. Veh. Engine Des., Vienna: Springer; 2016:117-146. https://doi.org/10.1007/978-3-7091-1859-7_8

[23] HP Academy. Which standalone ECU is the best? 2026. https://www.hpacademy.com/technical-articles/which-standalone-ecu-is-the-best/

[24] Jacob J, Colin JA, Montemayor H, Sepac D, Trinh HD, Voorderhake SF et al. InMotion: Hybrid race car, beating F1 at LeMans. 2013 Eighth Int Conf Exhib Ecol Veh Renew Energ. EVER, Monte Carlo: IEEE; 2013:1-16. https://doi.org/10.1109/EVER.2013.6521638

[25] Jones G. Engine of the Week: NASCAR Cup series Chevrolet 5.8L V8 engine. T2 Tomorrow's Technicians. 2017. https://www.tomorrowstechnician.com/engine-week-nascar-cup-series-chevrolet-5-8l-v8-engine/
[26] Kalociński T, Rymaniak Ł, Fuć P. Powertrain technology transfer between F1 and the automotive industry based on Mercedes-Benz. Combust Engines. 2020;172:3-13. https://doi.org/10.19206/CE-2018-101
[27] Lehbrink I. Stage set for the Class 1 era: a detailed look at the new BMW M4 DTM. 2018. https://www.press.bmwgroup.com
[28] Link ECU. Official ECU of Formula Drift. 2020. https://linkecu.com/2020-08-28-linkecu-official-ecu-of-formula-drift/
[29] Long-term reliability of the G16E-GTS. Toyota GR Corolla forum – ownership discussion. 2022. https://www.grcorollaforum.com/threads/long-time-reliability-g16e-gts.396/page-9?tl=pl
[30] Magda M. Mercedes AMG shows of F1 engine. Engine Labs. 2025. https://www.enginelabs.com/news/mercedes-amg-shows-off-f1-engine-hear-it-run/
[31] Martyr A, Martyr A, Plint M. Engine testing: The design, building, modification and use of powertrain test facilities. Elsevier; 2012.
[32] Papadakis. Racing – official website. 2026. https://doi.org/https://papadakisracing.com/
[33] Racing B. 2JZ GTE Turbo – 1700 HP street/strip engine complete Toyota Supra 3.2 L. Brangers Racing. https://brangersracing.com/shop/ols/products/206823150-2jz-gte-turbo-1700-hp-street-strip-engine-complete-toyota-supra-3-0-3-2-3-4
[34] Rotax Racing. 125 MAX / DD2 EVO products. 2026. https://www.rotax-racing.com/products/125-max-dd2-evo
[35] Silvestro B. Watch an 11,000-HP dragster engine get rebuilt in seven minutes. Road & Track. 2018. https://www.roadandtrack.com/motorsports/a23115209/top-fuel-dragster-v8-engine-rebuild/
[36] Stępień Z. A new generation of F1 race engines – hybrid power units. Combust Engines. 2016;167:22-37. https://doi.org/10.19206/CE-2016-403
[37] Sylt C. Revealed: The $1.4 billion cost of developing F1 engines. 2019. https://www.forbes.com/sites/csylt/2019/11/10/revealed-the-14-billion-cost-of-developing-f1-engines/
[38] Technology RE. Lamborghini Huracan GT3 naturally aspirated V10 GT3. Race engine technology. 2022. https://www.raceenginetechnology.com/News/lamborghini-huracan-gt3-naturally-aspirated-v10-gt3
[39] Venturoli E. The engine used in IndyCar competitions. RTR Sports. 2025. https://rtrsports.com/en/blog/the-engine-used-in-competitions-indycar/
[40] Zhang W, Wang B, Barber G, Lamonaca G. Low friction coating for high temperature bolted joints in IC engines. SAE Technical Paper 2023-01-0733. 2023. https://doi.org/10.4271/2023-01-0733

Filip Szwajca, DEng. – Faculty of Civil and Transport Engineering, Poznan University of Technology, Poland.
e-mail: *filip.szwajca@put.poznan.pl*

Prof. Ireneusz Pielecha, DSc., DEng. – Faculty of Civil and Transport Engineering, Poznan University of Technology, Poland.
e-mail: *ireneusz.pielecha@put.poznan.pl*

Łukasz Pajor, Eng. – Faculty of Civil and Transport Engineering, Poznan University of Technology, Poland.
e-mail: *lukasz.pajor@student.put.poznan.pl*

Grzegorz Marcisz – Gregor Performance Garage, Poland.
e-mail: *grzesiek1721@interia.pl*